IEEE Access
Multidisciplinary ⋮ Rapid Review ⋮ Open Access Journal

Received 17 January 2024, accepted 15 February 2024, date of publication 19 February 2024, date of current version 26 February 2024.

Digital Object Identifier 10.1109/ACCESS.2024.3367288

RESEARCH ARTICLE

Neural Network-Based Adaptive PID Controller Design for Over-Frequency Control in Microgrid Using Honey Badger Algorithm

AHMED H. YAKOUT[1], MASOUD DASHTDAR[2], KAREEM M. ABORAS[3], YAZEED YASIN GHADI[4], AHMED ELZAWAWY[5], AMR YOUSEF[6,7], (Member, IEEE), AND HOSSAM KOTB[3]

[1]Department of Electrical Engineering, Faculty of Engineering, Ain Shams University, Cairo 11517, Egypt
[2]Department of Electrical Engineering, Faculty of Sciences and Technologies Fez, Sidi Mohamed Ben Abdellah University, Fes 30000, Morocco
[3]Department of Electrical Power and Machines, Faculty of Engineering, Alexandria University, Alexandria 21544, Egypt
[4]Department of Computer Science and Software Engineering, Al Ain University, Abu Dhabi, United Arab Emirates
[5]Department of Electrical Engineering, Faculty of Engineering, Benha University, Shubra, Cairo 11629, Egypt
[6]Engineering Mathematics Department, Faculty of Engineering, Alexandria University, Alexandria 21544, Egypt
[7]Electrical Engineering Department, University of Business and Technology, Jeddah 23435, Saudi Arabia

Corresponding authors: Hossam Kotb (hossam.kotb@alexu.edu.eg) and Amr Yousef (a.yousef@ubt.edu.sa)

ABSTRACT Secondary frequency control systems, such as Automatic Generation Control (AGC), are used in interconnected power grids. However, when a system failure causes systems to separate into zones (islands), AGC can no longer be used, and the primary frequency control is the only control available. Moreover, load changes may cause frequency drop in some areas and over-frequency in other areas. Therefore, the goal in this article will be to design a neural network-based proportional, integral, and derivative (PID) controller in the primary control architecture to control the over frequency condition. The proposed controller is adaptively optimized in two stages by the honey badger algorithm (HBA). In the first stage, the PID controller gain values are optimized by the HBA algorithm for different values of load loss. While in the second stage, a feed-forward artificial neural network (ANN) is trained to match the tie-line measured power to the corresponding optimized HBA-PID gains obtained in the first stage. Finally, the proposed controller is implemented on a two-area interconnected thermal power system. The proposed controller results qualitatively outperform one of the best tuning methods, the Ziegler-Nichols (ZN) approach, and they show that the proposed controller has better dynamic responses with minimal frequency deviations and fast settling time, creating and guaranteeing a margin of stability for the closed loop.

INDEX TERMS Primary control, over frequency control, PID controller, ANN, honey badger algorithm, two-area system.

ABBREVIATIONS

AGC	Automatic Generation Control
PID	Proportional–Integral Derivative
HBA	Honey Badger Algorithm
ANN	Artificial Neural Network
ZN	Ziegler-Nichols
PSO	Particle Swarm Optimization
LP	Low-Pressure
IP	Intermediate-Pressure
HP	High-Pressure
CV	Control Valves
IV	Intercept Valves
MHC	Mechanical-Hydraulic Control
IVOB	IV Opening Bias
MLP	Multi-Layer Perception

LIST OF SYMBOLS

T_1	Transfer function of the inlet steam chest
T_2	Transfer function of the reheater
T_3	Transfer function of the crossover

The associate editor coordinating the review of this manuscript and approving it for publication was Wanqing Zhao.

T_{CH}	Time constant of the inlet steam chest
T_{RH}	Time constant of the reheater
T_{CO}	Time constant of the crossover
Pm	Mechanical power
T_{SR}	Time constant of the speed relay
T_{SM}	Time constant of the control valve servo motor
T_{SI}	Time constant of the intercept valve servo motor
K_G	Proportional controller gain
$\Delta\omega$	Rotor speed error
L_{I1}, L_{I2}	Open and close rate range of IV
L_{C1}, L_{C2}	Open and close rate range of CV
V_1	Setting value for over-speed limit
K_{AX}	Auxiliary governor gain
ω_i	Rotor speed
Pe	Electrical power
Hi	Inertia constant
D	Damping constant
R	Percentage of governor loss
R_T	Equivalent drop
$Xsys$	System state variable vector
$Ysys$	System output
$Usys$	Control input
J	Objective function
q	The weight assigned to distinct states
r	The weight assigned to control channels
P_{GV}	Power of governor
P_{HP}	Power of HP
P_{IP}	Power of IP
P_{LP}	Power of LP
ω	The rotational speed of the machine
P_{ref}	Load reference set point
x_{new}	HBA new location
x_{prey}	Prey position
F	The flag that promotes exploration
di	Distance between the prey and the i^{th} badger
r_1, r_2, r_3, *and* r_4	Random variables
α	Random control variable
β	The parameter of the ability to receive food
Ii	Intensity factor
P_{12}	Interrupted power
K_p, K_i, *and* K_d	PID controller coefficients
$W_{i,j}$	Weights of the output layer
$w_{j,l}$	Weights of the input layer
fj	Activation function of neuron j in the hidden layer
n_h	Number of neurons in the hidden layer
n_φ	Number of neural network inputs
Tij	Tie line synchronism coefficient
Tg	The time constant of the governor
Tt	The time constant of the steam turbine
Kr	Steam turbine reheater constant
Bg	Gas turbine valve position
Xg	Gas governor leading time constant
Yg	Gas governor lagging time constant
Tcr	Gas turbine ignition system reaction time delay
Tf	Gas turbine fuel time constant
Tcd	Gas compressor discharge time constant

I. INTRODUCTION

The main goal of a power network is to efficiently produce and distribute electrical power to end-users, while simultaneously upholding established criteria for electrical power quality. Two of the key criteria to consider are keeping the network frequency in close range to the nominal value and guaranteeing an uninterrupted supply of energy to consumers. Power from electricity is a particular resource that requires a constant balance between both production and consumption. Alternatively, any variations in network frequency can lead to instability and may end in serious damage to network infrastructure, including turbines, motors, transformers, and other related devices. Hence, to maintain the balance between power generation and consumption and to ensure that the network frequency maintains proximity to the required nominal value, specific control and safety procedures are used [1], [2], [3]. The initial control operation utilized to achieve this purpose is referred to as primary frequency control, while tertiary as well as secondary control act as additional controls in this respect [4], [5], [6]. The properties of primary and secondary frequency control, spanning their dynamic behavior and necessary conditions, are reliant on a variety of variables. These variables, which are fundamental to the system, exhibit diversity among different networks [7], [8], [9], [10]. Among the variables in consideration, the network inertia constant, the load's frequency dependency, and the speed and quantity of units engaged in frequency control, along with their available capacity, emerge as the most crucial factors influencing the operation and control of the network frequency [11], [12], [13].

Due to the wide dimensions of the power system, it is not possible to control it centrally in the form of an integrated system, and in practice, control plans are designed and implemented hierarchically [14], [15]. For example, for load-frequency management, the control of the first layer is done through the governors in the generation unit and without the need for a central controller, and the control of the second layer is done through the automatic generation control with the help of setting the reference of the governors of several generation units in one area. For the control of the next layers, the range of control is widened and the time constant of the controllers is increased to avoid interference of the controllers. Unlike the voltage range, the frequency is almost the same at all points of the power system in a steady state. Unbalance of active power due to events such as sudden load change or entry and exit of generation units will lead to a frequency deviation. Therefore, multi-area power systems should be able to control the frequency changes and stabilize them at a certain value through the control

units of each area and interaction with the units of other areas [16], [17], [18]. The relationship that exists between the frequency in the electrical system and the spin rate of the generator provides a direct connection between frequency control and the monitoring of the turbine-generator unit's speed. The original implementation of speed control involved the incorporation of a governor system, that detected the machine's speed and adjusted the input valve accordingly to modify the mechanical power output. This adjustment is made to effectively respond to changes in the load and return the frequency to its designated nominal value. The load frequency control system consists of three parts regulating the speed of the steam turbine and the inertia of the system, and to increase the efficiency of the thermal cycle and the useful life of the turbine blades, multi-story turbines are used. In this control system, by opening or closing the steam valve, the steam flow on the turbine is regulated and finally controls the output active power of the generator [19], [20], [21], [22], [23].

After the occurrence of failures such as the exit of one of the power generation units of the network, separation of some areas, or a sudden change in the network load that causes the balance between generation and consumption to be disrupted, the power networks will experience sudden changes in their frequency. These increasing or decreasing changes in network frequency are always considered one of the serious threats to the stability of this type of network. Therefore, examining and analyzing the frequency response of power systems in the moments after the occurrence of accidents is always proposed as the first step in planning to overcome this problem. Carrying out the differential equations of power generators in the time domain to calculate the rotation speed of generators is one of the methods that can be used in this field [24], [25], [26]. However, due to the very large computational volume of this method and the need for system operators for a simpler method to analyze the overall behavior of the network frequency, it is appropriate to use other methods to investigate and analyze the frequency response of the system. Therefore, defining the dynamic structure of power generators in the form of an integrated model along with filtering some unnecessary characteristics of the frequency response of the system is one of the best methods that can be used in this field. Therefore, estimating and examining the frequency response of power systems in the event of a sudden change in load, using accurate and fast models, is one of the most important issues that has always been the concern of the operators of these systems. One of these methods, first order and at the same time accurate models with the combination of PID controllers have been presented to investigate the overall frequency behavior of power networks. In addition, to simplify complex dynamic models, optimization, and planning problems of power plant units in the presence of frequency control constraints are used. The use of such models can create a linear space in the frequency relationships of these problems and, accordingly, reach the optimal answer quickly and more precisely [27], [28], [29], [30], [31], [32], [33].

In the recent past, plenty of investigation has been undertaken to improve the frequency stability of power systems by optimizing the control parameters, in which the PID controller has been used the most. In [34], an optimized PID controller was presented using Kharitonov's theorem to control the load frequency, in [35], the quadratic regulator approach with compensating pole technique was used to design an optimal PID controller, in [36] a PID control approach based on linear matrix inequality, in [37], a new technique for FOPID controller design is presented, which uses the Big Bang Big Crunch algorithm and internal model control. Most PID controllers have been combined with fuzzy systems [38], [39], [40], [41], [42], PSO [43], [44], [45], [46], or designed using artificial neural networks (ANN) [47], [48], [49], [50], [51]. Many controllers from the PID family have been discussed in different references to solve the problem of automatic frequency control in power systems and improve the system response. Since the set of power systems is a non-linear system and it is not possible to express a precise mathematical model for it, in recent years, neural network systems have been used as controllers to cover these uncertainties and non-linearities. In [52], to maintain the voltage-frequency stability of the power system, an ANN-based PD controller is used and its results are compared with the magnetotactic bacteria optimization algorithm. In [53], to maintain the network frequency within the allowed range due to resonance attacks, ANN based on an observer sliding mode controller is used, in which resonance uncertainties are considered as input and it is tried to use ANN to detect and reduce them. In [54], the neural PID controller is used to control the frequency of the network, where the ANN consists of three hidden layers with 15 neurons, and its results are compared with the fuzzy controller. In [55], to control the frequency of the two-area system, ANN was used to optimize the PID controller, and considering the challenges of ANN training, the PSO algorithm was used to reduce the mean squared error criterion for ANN training. In [56], in addition to ANN, intelligent algorithms such as modified particle swarm optimization with PI-PD controller are used to control the voltage frequency of the network. Although the presented methods have a good performance in frequency control, most of the aforementioned methods are only suitable for a situation where the network parameters and components do not change, and if there is a change in these values, these types of controllers must be adjusted again through new test data. In this type of controller, there are problems such as a large number of inputs for training the network how to choose the number of neurons in the middle layer, and increasing the calculation time for online tasks. But it seems that if we can create a fully adaptive controller that uses the information of every moment of the system and according to the changes in the operating points for the control problem, the performance of the controller can be improved by quickly

adjusting the control gains. One way to solve this problem is to train ANN online using meta-heuristic algorithms in such a way that for each change in the network through these algorithms, in addition to controller optimization, ANN can also be trained. Another challenge of such methods occurs against a sudden drop in load due to the interruption of one area and the increase of generation in another area, because in this case, the problem of over-frequency has occurred, which will be an unpredictable problem. Therefore, a special provision should be made to control it.

In this article, a Neural Network-based adaptive PID controller for over-frequency control is presented, which uses the HBA algorithm (which is an algorithm with fast and effective search in the problem space and creating interaction between steps) to optimize and train the controller. In such a way, the proposed controller is designed in two stages. In stage 1, the gain values of the PID controller were optimized by HBA for different values of loss of load (i.e., different values of interrupted tie line export power), while in stage 2, a feed-forward ANN is trained to match the tie line power measured to the corresponding HBA-PID gains obtained in stage 1. So, the neural network would change the gains of the PID controller based on the pre-fault value of the tie-line power exported. The gains produced by the neural network are nothing, but the HBA gains optimized in stage one. Consequently, the PID responds adaptively as the PID gains change with operating conditions. Hence, the main contributions of this work are:

- Over-frequency control in islanded microgrid using a Neural Network-based adaptive PID controller.
- Using the HBA algorithm to optimize the PID controller at different load loss values.
- Applying the corresponding HBA-PID parameters to train a feed-forward ANN thus obtaining an adaptive HBA-based neural network capable of changing the PID parameters according to the value of load loss.

The following parts of the paper are summarized as follows: The first section provides an introduction, while the second section presents a background on the issue of over-frequency in power systems. The third section then discusses a case study along with the first simulation results. The fourth section of the paper introduces trains, validates, and simulates the suggested self-tuning control technique using the HBA algorithm. Finally, the fifth section concludes this piece of work.

II. EXPLANATION OF THE OVER-FREQUENCY PROBLEM AND ITS CONTROL INFRASTRUCTURE

Figure 1 shows an interconnected power system consisting of steam turbine generators, where the tie-line is the connection between areas 1 and 2. It can be seen that P12 is the power transferred from area 1 to area 2. Suppose that area 2 is separated from area 1 due to a fault. In this case, area 2 is faced with a lack of generation, and as a result, a frequency drop occurs in area 2, while area 1, is faced with a sudden drop in load, and due to the excess generation, the frequency of

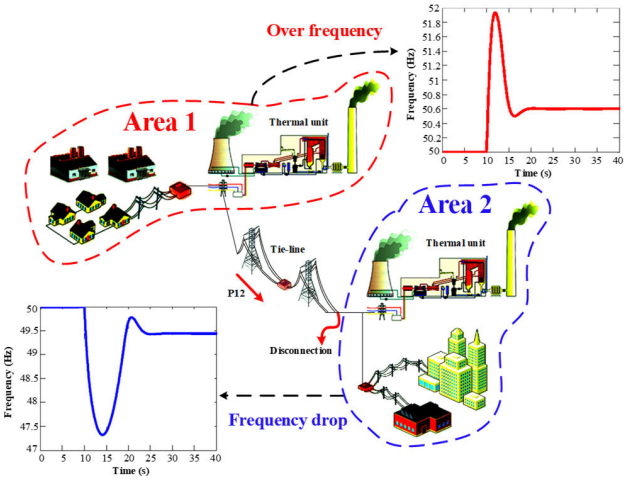

FIGURE 1. Frequency changes in the areas of interconnected power systems in island mode.

area 1 increases, and in the term, over frequency occurs. The discussion in this article is to study and present a new method for over-frequency control in steam turbines. According to the standard, in the over-frequency state, the frequency swings should be damped quickly, and the frequency overshoots should not be more than 4% of the nominal frequency value (52 Hz for a 50 Hz system), otherwise, the generating unit protection system trip command will be issued. In the following section, steam turbine components are modeled, and the conventional frequency control structure and how to determine its parameters are described.

A. MODELING OF STEAM TURBINE COMPONENTS

The steam released in the boiler is utilized to propel the turbine in a steam turbine system. The high-pressure steam is expanded inside a nozzle, and a part of its thermal energy is converted into kinetic energy. By adhering to the principles of reaction, this kinetic energy is then transformed into mechanical energy. For steam turbines, to be more efficient, there is a part called a reheater, in which the steam is returned to the boiler after expansion and is reheated to the initial temperature, then this steam is returned to the turbine for expansion in the final stage of the turbine. Another part that is located at the output of the steam turbine is the condenser which works under a vacuum, which causes the difference between the input and output pressure to produce more turbine energy. In this way, they keep the cooling system under vacuum and increase the pressure difference by minimizing the output pressure. The exhaust steam of the turbine, which is sucked into the cooler by the vacuum system, is cooled by water and turned into distilled water, and it is used to make steam again. To make full use of steam energy, three turbine stages: the low-pressure (LP) turbine, intermediate-pressure (IP) turbine, and high-pressure (HP) turbine have been considered. The turbine shaft is connected to the generator shaft. So, when the turbine shaft moves, the generator rotates and electrical energy is produced. During

this process, the steam loses its energy. Then the saturated low-pressure steam passes through the condenser and turns into a liquid. After that, the water is directed to the pumps of the first stage and the cycle is complete. Therefore, this cycle is constantly repeated to produce energy. Figure 2 shows the block diagram and component model of a single reheat tandem-compound steam turbine.

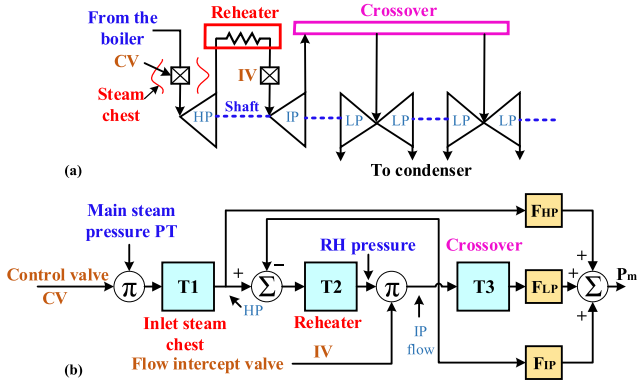

FIGURE 2. Single reheat tandem-compound steam turbine model. (a) Turbine configuration and (b) Block diagram representation.

As seen in Figure 2(a), initially, the steam is introduced into the high-pressure (HP) portion via a series of valves known as control valves (CV). Subsequently, the high-pressure exhaust steam undergoes a process of reheating within the reheater section and subsequently proceeds into the intermediate-pressure (IP) turbine section via a distinct set of valves known as intercept valves (IV). Due to the high steam levels in the reheater section, rapidly closing the CV valves will not be sufficient to address the over-speed issue with the over-frequency problem. Typically, control valves are employed to modulate the frequency. Therefore, for the problem of over-frequency, the best performance is to use IV valves that control the steam flow of IP and LP sections ahead of the reheater section. This part produces almost 70% of the total power of the turbine. In Figure 2(b), the inlet steam chest, reheater, and crossover models are shown with transfer functions T_1, T_2, and T_3, respectively as follows [52], [53], [54], [55], [56]:

$$T_1 = \frac{1}{1 + sT_{CH}} \tag{1}$$

$$T_2 = \frac{1}{1 + sT_{RH}} \tag{2}$$

$$T_3 = \frac{1}{1 + sT_{CO}} \tag{3}$$

where T_{CH}, T_{RH}, and T_{CO} are the time constants of the inlet steam chest, reheater, and crossover, respectively. The power of HP, LP, and IP turbines is shown in Figure 2(b) with fractions F_{HP}, F_{LP}, and F_{IP}, respectively. One of the important parts of a steam turbine in frequency control is the governor, which is shown in Figure 3 functional block diagram of a mechanical-hydraulic control (MHC) system in the structure of a steam turbine. As you can see in Figure 3(a), the speed output of the governor is compared with the speed/load reference. This reference is determined by the state of the speed changer. Finally, this obtained error signal is used to control CV and IV valves. The IV valve is controlled by the opening bias (IVOB) signal and is usually kept fully open, but in the over-speed position due to the large speed error signal created, the IVOB is removed, and the IV valves close quickly. Finally, when the restored control signal reaches a value lower than IVOB, the IV valves are fully opened again. In Figure 3(b), T_{SR}, T_{SM}, and T_{SI} are the time constants of the speed relay, control valve servo motor, and intercept valve servo motor, respectively. Also, KG is the proportional controller gain related to the generator's rotor speed and its rotor speed error ($\Delta\omega$). Here, L_{I1} and L_{I2} are the open and close rate range of IV, respectively. While L_{C1} and L_{C2} are the CV servo motors, respectively. Moreover, one of the conventional parts of the MHC system used to limit over-speed is the auxiliary governor, and when the speed exceeds the set value of V_1, it is activated in parallel with the main governor with KAX gain and can effectively increase the gain of the speed control loop. In this case, to limit over-speed, CV and IV valves are closed quickly. Although this high gain auxiliary governor limits the frequency maximum overshoot, it causes the valves to open and close repeatedly near nominal frequency leading to the sustained oscillation at a steady state.

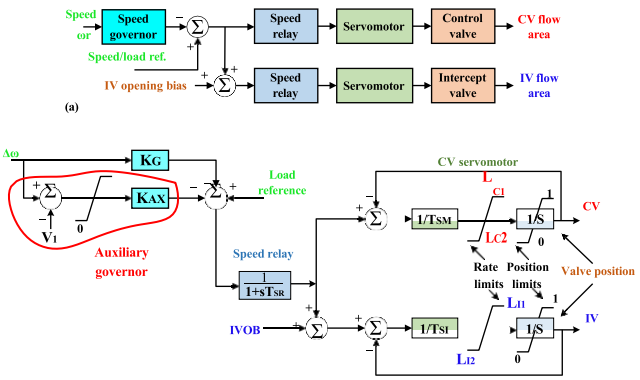

FIGURE 3. MHC turbine-governing system model. (a) Functional block diagram of MHC and (b) Governing system with intercept valve.

B. THE CONVENTIONAL STRUCTURE OF OVER-FREQUENCY CONTROL BASED ON STATE EQUATION ANALYSIS IN ISLAND MODE

Proper control of the network against disturbances and smooth or sudden load changes requires knowledge of the system and its accurate modeling. However, it is unnecessary to model all the details of the network to study the effects of sudden overload or load removal in the network, because the speed of the secondary and tertiary loops is so low that they practically do not play a role during the transients. In addition, it is not necessary to model the details and fast transients, as well as phenomena and slow network controllers that are not effective in the primary frequency control in the studied period. Therefore, the effect of inter-machine oscillations

and transmission systems is not considered in the primary frequency control. In generator- turbine i, the relationship between the input-output power and its frequency will be as Equation (4) according to the fluctuation equation per unit [52], [53], [54], [55], [56].

$$2H_i \frac{d\omega_{i(pu)}}{dt} = T_{acci} = T_{mi} - T_{ei} = P_{mi} - P_{ei} \tag{4}$$

where ω_i is the speed of the rotor in terms of p.u., P_{mi} is the mechanical power supplied by the turbine, P_{ei} is the electrical power of the generator output and H_i is the inertia constant in seconds. Equation (4) around the working point can be written as Equation (5) for electrical and mechanical power changes. Assume M = 2H [52], [53], [54], [55], [56].

$$M_i \frac{d\Delta\omega_{i(pu)}}{dt} = \Delta P_{mi} - \Delta P_{ei} \tag{5}$$

In general, the system load consists of a wide range of loads, including loads of resistive, heating, lighting, motor, etc. For motor loads, including fans and pumps, the number of consumption changes with the change of frequency and, as a result, the change in the speed of the motors. Therefore, system load changes will include a component proportional to the frequency change and an independent component as Equation (6). Here, D is the load-damping constant or load-frequency sensitivity coefficient [52], [53], [54], [55], [56].

$$\Delta P_L = \Delta P_{L0} + D\Delta\omega,\ D = \frac{\partial P_L}{\partial \omega} \tag{6}$$

Figure 4 depicts a simplified power system frequency model where the total mechanical outputs of separate turbines drive all the generators as an equivalent generator with an inertia constant equal to M_{eq}. The corresponding generator speed represents the system frequency in this case. According to Figure 4 and taking the Laplace transform, we reach the final Equation (7) for system frequency changes. where ΔP_m is the total power produced by network generators and ΔP_e is the total electric load received from the generators [52], [53], [54], [55], [56].

$$\begin{aligned} \Delta\omega(s) = \Delta f(s) &= \frac{\Delta P_m(s) - \Delta P_e(s)}{M_{eq}s + D}, \\ \Delta P_m &= \sum\nolimits_i \Delta P_{mi} \\ \Delta P_e &= \sum\nolimits_i \Delta P_{ei} \end{aligned} \tag{7}$$

Since the study is on steam turbines, according to the details provided in section II-A, by modifying Figure 4, the closed-loop primary frequency control mechanism can be shown in Figure 5. The variable R is the characteristic of the unit or the percentage of governor loss and shows the dependence of the change of the unit's generation power on the frequency changes in the steady state.

To participate units according to their rated power in frequency control, the value of R is usually considered to be almost the same for all generation units of a network and in the range of 3 to 7%. In steady state, for a network and the i^{th}

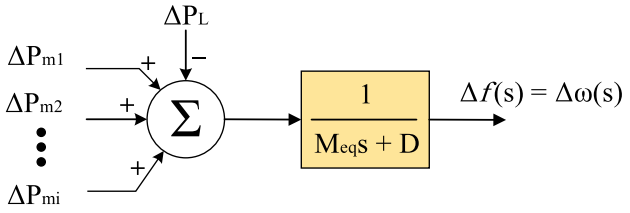

FIGURE 4. A simple frequency model with the equivalent generator.

unit, we will have Equation (8) [52], [53], [54], [55], [56]:

$$\frac{\Delta f}{f_n} = -R_i \frac{\Delta P_{mi}}{P_{ni}} \tag{8}$$

Here, the index n represents the nominal value. As a result, the change in the total generation power of the system that has several participating units in frequency control is expressed as Equation (9) [52], [53], [54], [55], [56]:

$$\Delta P_T = \sum\nolimits_i \Delta P_{mi} = -\frac{\Delta f}{f_n} \sum\nolimits_i \frac{1}{R_i} P_{ni} \tag{9}$$

From Equation (9), the equivalent drop (R_T) for a network with several generation units can be obtained as Equation (10) [52], [53], [54], [55], [56].

$$R_T = \frac{\sum_i \Delta P_{mi}}{\sum_i \frac{1}{R_i} P_{ni}} \tag{10}$$

If an imbalance in the form of ΔPL(s)= ΔPL/s is applied to the system, then the relationship governing the frequency behavior of the system for Figure 5 will follow from Equation (11), as shown at the bottom of the next page.

One of the conventional methods in frequency control is to use the analysis of the state space equations according to the dynamic behavior equations governing the over-frequency pattern of the system in Figure 5. The state space pattern for each island area with steam turbine i, with decentralized design, is described as a set of Equations (12), where X_{sys} is the system state variable vector, Y_{sys} is the system output, which here represents the frequency of the area ω, and in Finally, Usys will be the system inputs.

$$\begin{aligned} \dot{X}_{sys} &= A_{sys}X_{sys} + B_{sys}U_{sys} \\ Y_{sys} &= C_{sys}X_{sys} \end{aligned} \tag{12}$$

The purpose of this study is to develop an optimum controller that minimizes the objective function shown in Equation (13) for the control input U_{sys}. Function J denotes the aggregate of state and control energy, with q and r representing the corresponding weights assigned to distinct states and control channels, respectively as shown in Eq. 13. When the value of r is significantly more than q, the control energy experiences a substantial penalty. Consequently, the implementation of the control rule necessitates the utilization of small motors, actuators, and amplifiers. Conversely, when the value of q far exceeds that of r, the state experiences a substantial penalty, leading to a system characterized by significant damping.

$$J = \frac{1}{2} \int_0^T qX^2 + rU^2 dt \tag{13}$$

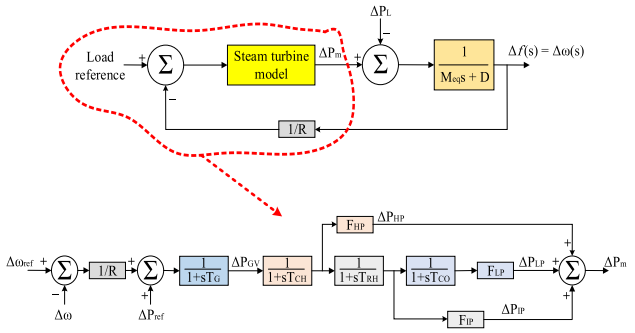

FIGURE 5. Frequency model with a steam turbine.

As a result, according to the identification and determination of system dynamics through states: P_{GV}, P_{HP}, P_{IP}, P_{LP}, and ω in Figure 5, Equation (12) can be expressed as Equation (14), as shown at the bottom of the next page, about the dynamic pattern of the area under study. Eventually, given the primary objective of enhancing the frequency response of the steam turbine, the sole output of the system is the rotational speed ω of the machine. Hence, the goal function can be expressed by Equation (15), as shown at the bottom of the next page. Where P_{ref} represents the governor speed changer or load reference setpoint.

III. CASE STUDY AND SIMULATION RESULTS WITH CONVENTIONAL CONTROL

This article presents an evaluation of the performance of the suggested controller in various scenarios, comparing it with conventional methods on Kundur's two-area power system. Figure 6 depicts the power system in this model, which consists of two similar sections linked by a tie line. Every section comes with a pair of identical 20 kilovolt/900 megavolt-ampere, 50 Hz generators. Every generator is supplied with a static exciter and an inclusive prime mover. The power capacity of area 1 exhibits a range of 67 to 1267 MW, whereas the power capacity of area 2 ranges from 1467 to 2667 MW. Area 1 allows the transmission of electrical power to Area 2 by the use of two 220 kV tie lines. Once any line is tripped for any reason, the other line will be overloaded and will trip as well causing the disconnection of Area 1 from Area 2. Consequently, the frequency of Area 1 is going to experience an increase correlated to the magnitude of power being exported. Furthermore, Table 1 presents relevant information on the system being investigated.

Initially, the performance of conventional techniques for over-speed control, such as the intercept valve and auxiliary governor, is discussed to gain a better understanding of the performance of the suggested PID controller. As suggested by the intercept valve technique, the use of high-speed valves

TABLE 1. Information about the power system.

Generator parameters in per unit				
X_d=1.8	X_q=1.7	X_l =0.2	X'_d= 0.3	X'_q= 0.55
X''_d=0.25	X''_q=0.25	R_a=0.0025	T'_{d0}=8.0s	T'_{q0}=0.4 s
T''_{d0}=0.03s	T''_{q0}=0.05 s	H=4 s		
Transformers 20/500 kV				
Transformer impedance = j0.15 per unit on 1000 MVA base				
The transmission line parameters				
R = 0.0001 pu/km	X_L = 0.001 pu/km		B_C = 0.00175 pu/km	
Governing system parameters				
K_G = 20	T_{SR} = 0.7 s	T_{SM} = 0.23 s	T_{SI} = 0.23 s	L_{CI} = 1.0
L_{C2} = -3.0	L_{I1} = 1.0	L_{I2} = -2.5	F_{HP} =0.3 s	F_{IP} = 0.3 s
F_{LP} = 0.4 s	IVOB = 1.17	K_{AX} = 149	V_1 = 0.02	

at the outlet of the reheater serves to impede the flow of steam toward the intermediate-pressure and low-pressure turbines during instances of excessive rotational speed. Consequently, the output power is decreased. Also in the auxiliary governor technique, a high-value P controller comes into action once the frequency exceeds 2%. Figure 7 shows how to model prime mover in MATLAB software. Now the performance of this model is evaluated with different load loss percentages in Area 1. Figure 8 shows the performance results of traditional techniques in reducing network frequency overshoot for different load loss percentages in Area 1. Two important factors in over-frequency control are the rapid reduction of overshoot and being below 52 Hz and the reduction of frequency fluctuations and being in a steady state. As you can see in Figure 8, at first the intercept valve came into action and reduced the severity of the frequency overshoot, and then the auxiliary governor performed better and reduced the frequency to some extent. In Figure 8(a), the overshoot was above 51.5 Hz, finally, the frequency reached below 50.5 Hz and reached a steady state within 30 seconds, in Figure 8(b), the overshoot was above 53 Hz, and finally, the frequency has reached below 51 Hz, but it continues to fluctuate for more than 40 seconds. In Figure 8(c) and (d), the overshoot is above 54 Hz, and similar to the previous two cases, it is still a fluctuating frequency and has not reached a steady state. Moreover, Figure 8(e) shows the percentage of frequency overshoot per load loss. As you can see, the auxiliary governor technique was able to keep the overshoot under 4% only up to 40% of load loss.

Therefore, it can be concluded that the conventional over-speed control cannot solve the over-frequency problem when the power loss exceeds 40% of the connected load, moreover, the traditional auxiliary governor introduces permanent frequency fluctuations. To solve this problem, in this article,

$$\Delta\omega(s) = \Delta f(s) = \Delta P_L(s)\left[-\frac{\frac{1}{M_{eq}s+D}}{1+\frac{1}{R_T}\left(\frac{1}{1+sT_G}\right)\left(\frac{1}{1+sT_{CH}}\right)\left[F_{HP}+\left(\frac{F_{IP}}{1+sT_{RH}}\right)+\left(\frac{F_{LP}}{(1+sT_{RH})(1+sT_{CO})}\right)\right]\left(\frac{1}{M_{eq}s+D}\right)}\right] \quad (11)$$

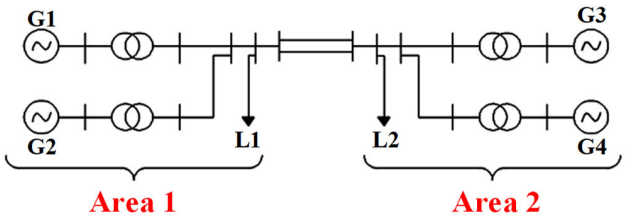

FIGURE 6. Two-area, four-machine system.

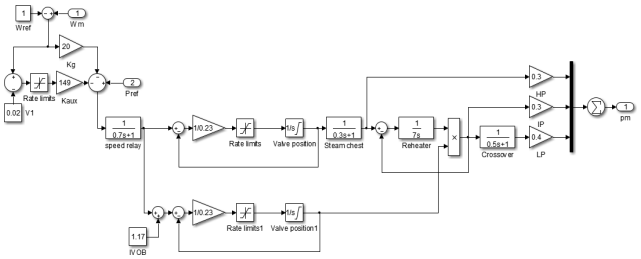

FIGURE 7. Prime mover with auxiliary governors.

it is proposed to use a Neural Network-based Adaptive PID controller using the HBA algorithm.

IV. DESIGN OF PROPOSED NEURAL NETWORK-BASED ADAPTIVE PID CONTROLLER USING HBA ALGORITHM

Although the auxiliary governor can be used to limit over-speed, the study shows that if the value of V1 in Figure 3 is not selected correctly, it will cause the instability of the speed control in the island state of the system and the system will be in fluctuating condition. Then the units on the island will respond to the oscillations of the units with the auxiliary governor. In the meantime, all the units will undergo oscillation, leading to the ongoing movement of the steam valves until the hydraulic systems of the governors deplete their oil supply. This depletion will result in the tripping of the unit and perhaps creating an electrical outage on the island. Therefore, according to Figure 9, in this article, it is suggested to use a prime mover with an additional PID controller instead of a conventional high gain proportional auxiliary governor. The structure of the proposed PID controller is designed based on a nonlinear artificial neural network (ANN) controller trained by the HBA algorithm. By using the proposed controller, it is possible to consider the limitations of the steam turbine variables systematically, but the use of this method requires an accurate model of the process, which was presented in the previous part of the necessary modeling. The suggested control system employs a feed-forward Multi-Layer Perception (MLP) neural network paradigm. The HBA approach is further utilized for training and optimization. The HBA method is described first, and then the various phases of developing the suggested PID controller are covered in depth.

A. HBA OPTIMIZATION ALGORITHM

The objective function is optimized in this article using the Honey Badger Algorithm (HBA). By moving fast over the search space and avoiding local optimal solutions, this algorithm aims to find a balance between the exploration and exploitation phases. Additionally, the HBA (Heuristic-based Algorithm) has demonstrated its effectiveness in addressing empirical challenges characterized by complex search spaces. The primary stages of the HBA algorithm are depicted in Figure 10 and may be simply outlined as follows [57]:

1) EXPLORATION PHASE (HONEY PHASE)

In this phase, the honey badger follows a honeyguide bird to a beehive and can be calculated as follows [57]:

$$x_{new} = x_{prey} + F \times r_1 \times \alpha \times d_i \tag{16}$$

where the optimal prey position is represented by x_{prey} and the honey badger's new location is indicated by x_{new}. The random number r_1 is a value between 0 and 1. Furthermore, the distance between the i^{th} badger and the prey is denoted by d_i which can be calculated as follows [57]:

$$d_i = x_{prey} - x_i \tag{17}$$

The density factor (α) regulates the randomization process over time to ensure smooth transition from exploration to exploitation. Furthermore, the variable α serves as a random control factor that has the effect of reducing the overall variety within the population. Its calculation may be determined

$$\begin{bmatrix} \Delta\dot{P}_{GV} \\ \Delta\dot{P}_{HP} \\ \Delta\dot{P}_{IP} \\ \Delta\dot{P}_{LP} \\ \Delta\dot{\omega} \end{bmatrix} = \begin{bmatrix} -1/T_G & 0 & 0 & 0 & -1/RT_G \\ F_{HP}/T_{CH} & -1/T_{CH} & 0 & 0 & 0 \\ 0 & F_{IP}/F_{HP}T_{RH} & -1/T_{RH} & 0 & 0 \\ 0 & 0 & F_{LP}/F_{IP}T_{CO} & -1/T_{Co} & 0 \\ 0 & 1/M_{eq} & 1/M_{eq} & 1/M_{eq} & 0 \end{bmatrix} \begin{bmatrix} \Delta P_{GV} \\ \Delta P_{HP} \\ \Delta P_{IP} \\ \Delta P_{LP} \\ \Delta\omega \end{bmatrix} + \begin{bmatrix} 1/T_G & 0 \\ 0 & 0 \\ 0 & 0 \\ 0 & 0 \\ 0 & -1/M_{eq} \end{bmatrix} \begin{bmatrix} \Delta P_{ref} \\ \Delta P_L \end{bmatrix}$$

$$[\Delta\omega] = \begin{bmatrix} 0 & 0 & 0 & 0 & 1 \end{bmatrix} \begin{bmatrix} \Delta P_{GV} \\ \Delta P_{HP} \\ \Delta P_{IP} \\ \Delta P_{LP} \\ \Delta\omega \end{bmatrix} \tag{14}$$

$$J = ISE = \frac{1}{2}\int_0^T q\Delta\omega^2 + r\Delta {P_{ref}}^2 dt \tag{15}$$

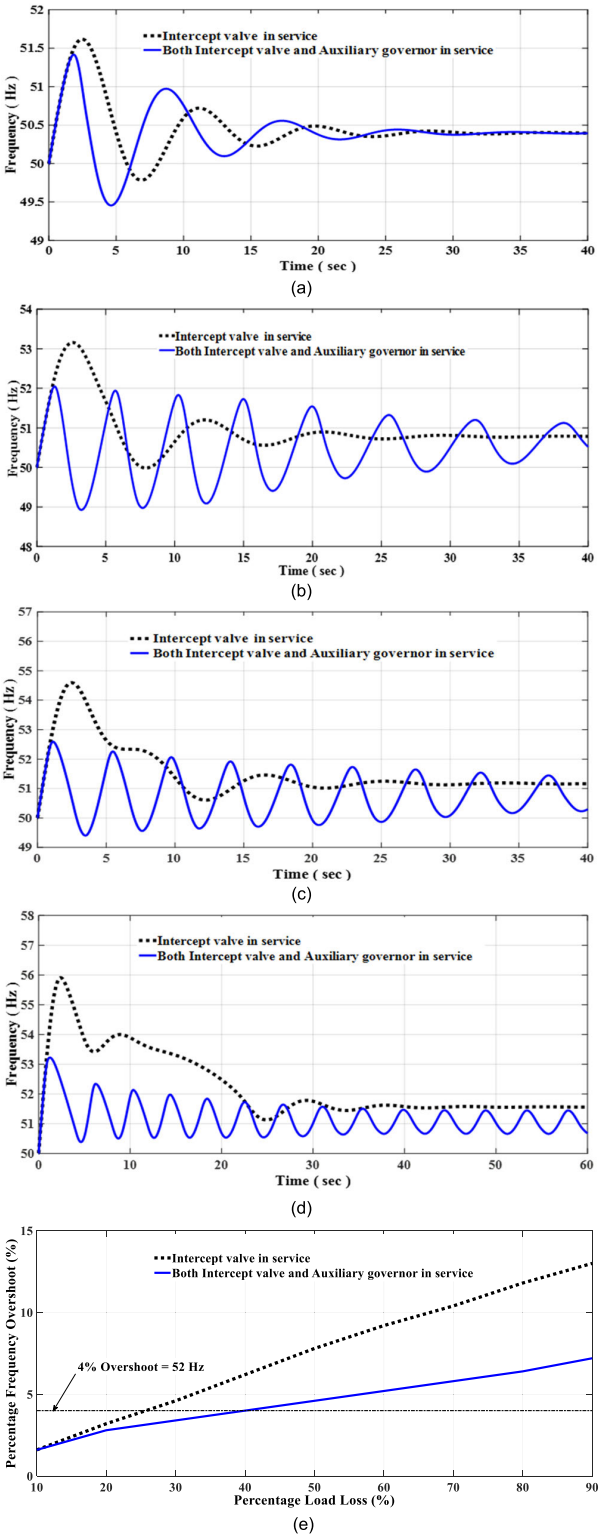

FIGURE 8. Frequency changes in case 1. (a) 20% of load loss in Area 1, (b) 40% of load loss in Area 1, (c) 60% of load loss in Area 1, (d) 80% of load loss in Area 1 and (e) Frequency overshoot versus load loss for traditional overspeed control.

by [57]:

$$\alpha = 2 \times exp\left(\frac{-t}{MaxIt}\right) \tag{18}$$

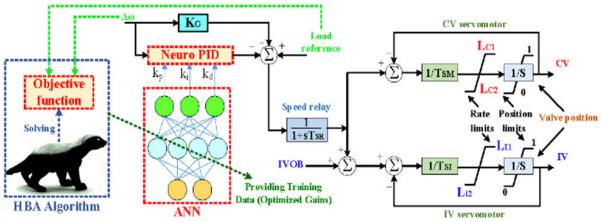

FIGURE 9. Prime mover with additional proposed PID controller.

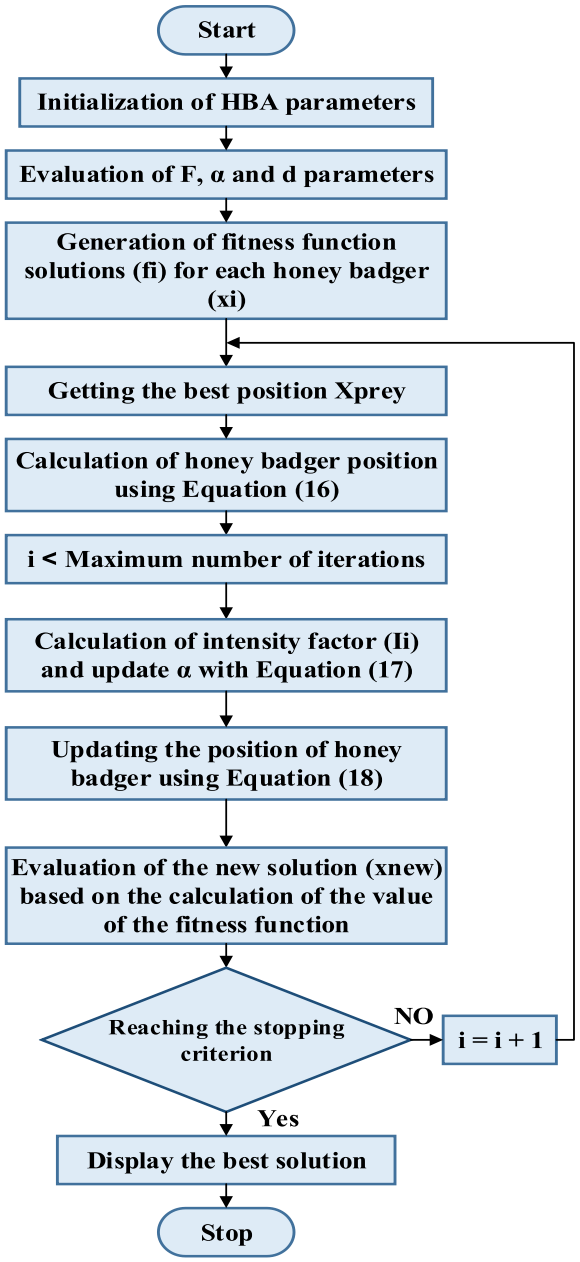

FIGURE 10. Flowchart of the HBA algorithm.

where t is the iteration number and ***MaxIt*** is the maximum number of iterations. F works as the flag that alters search direction and can be determined as follows [57], (19), as shown at the bottom of the next page.

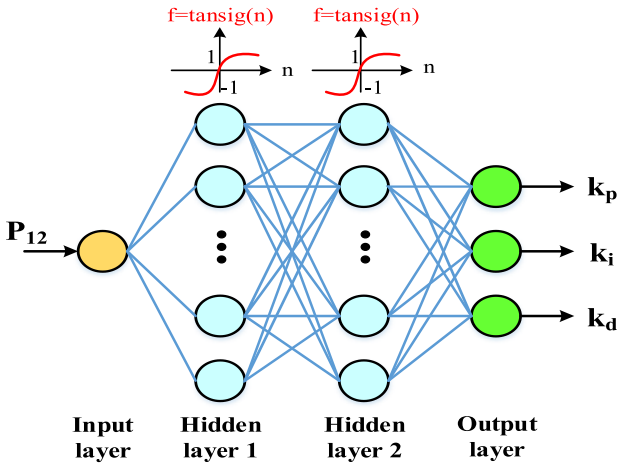

FIGURE 11. Schematic diagram of the construction of the adopted neural network model.

TABLE 2. Control parameters from ZN and HBA methods.

Load1 (MW)	P_{tie} (MW)	Load2 (MW)	Power interruption (%)	ZN method			HBA method		
				kp	ki	kd	kp	ki	kd
900	100	1100	10 %	19.95	7.98	12.46	38.79	10.76	41.70
800	200	1200	20 %	16.25	6.50	10.15	35.46	11.47	42.16
700	300	1300	30 %	16.25	6.50	10.15	34.78	8.54	42.76
600	400	1400	40 %	16.19	6.47	10.12	44.72	17.79	34.48
500	500	1500	50 %	16.19	6.47	10.12	43.28	24.47	26.35
400	600	1600	60 %	16.19	6.47	10.12	41.63	36.85	40.56
300	700	1700	70 %	17.10	6.84	10.69	35.18	32.09	45.88
200	800	1800	80 %	17.10	6.84	10.69	30.70	22.48	43.82
100	900	1900	90 %	17.10	6.84	10.69	38.42	12.03	39.57

2) EXPLOITATION PHASE (DIGGING PHASE)

In this phase, the honey badger digs in a cardioid-shaped motion and can be calculated as follows [57]:

$$x_{new} = x_{prey} + F \times \beta \times I_i \times x_{prey} + F \times r_3 \times \alpha \times d_i \times |cos(2\pi r_4) \times [1 - cos(2\pi r_5)]| \quad (20)$$

where the variable "I_i" represents the intensity factor, which is dependent upon the proximity between each pair of neighboring search agents as well as the distance between the prey and the honey badger. Moreover, r_3, r_4 and r_5 are represented by uniform random distributions that take a value between 0 and 1. The parameter β, denoting the foraging efficiency of the honey badger, was assigned a value of 6 in the current study [57]. The initial values of HBA are selected as follows [57]:

Honey badger number $= 50$, $MaxIt = 30$, $\beta = 6$, $r_1 = r_2 = r_3 = r_4 = r_5 = 0.5$ and $F = 1$. Moreover, the primary procedures of the HBA algorithm can be succinctly outlined as follows:

a. Initialize the number of search agents and their lower and upper boundaries.

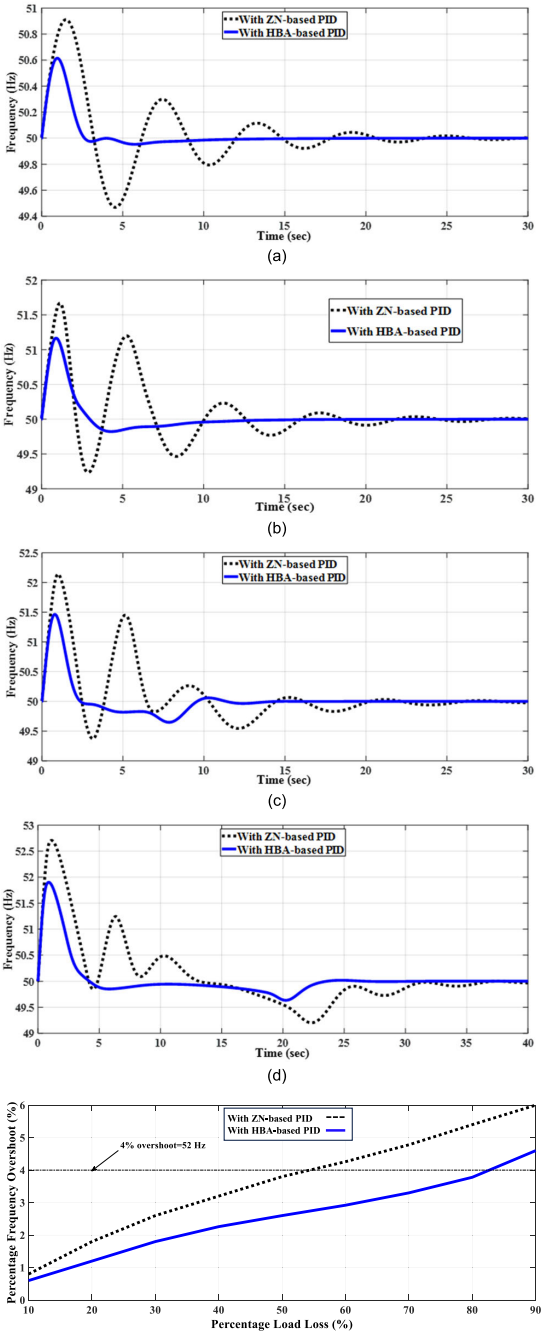

FIGURE 12. Frequency changes in case 2. (a) 20% of load loss in Area 1, (b) 40% of load loss in Area 1, (c) 60% of load loss in Area 1, (d) 80% of load loss in Area 1 and (e) Frequency overshoot versus load loss for ZN and HBA-based PID controllers.

$$F = \begin{cases} 1 \; if \; r_2 \leq 0.5 \\ -1 \; else, \end{cases}, \; r_2 \text{ is a random number between 0 and 1} \quad (19)$$

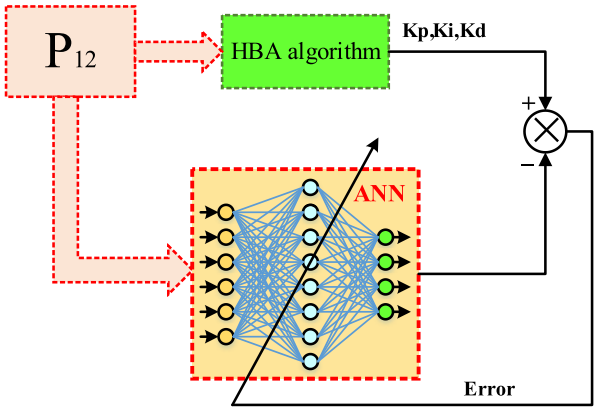

FIGURE 13. Block diagram of the proposed control system.

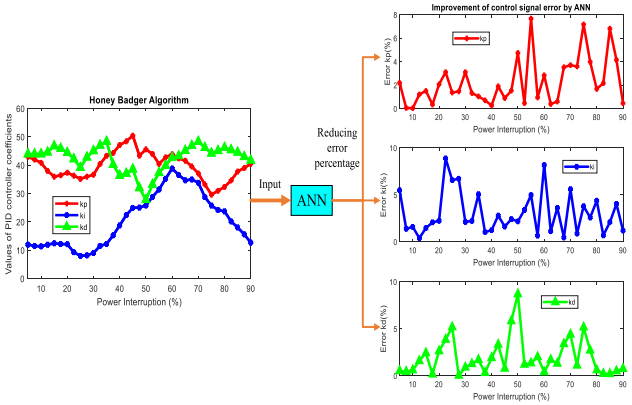

FIGURE 14. Percentage reduction of control signal error of coefficients k_p, k_i, k_d in case 3.

b. Define the intensity I_i which represents the prey strength and distance between the honey badger and the prey to determine the motion speed of the honey badger.
c. Update the density factor α to make a smooth transfer from the exploration phase to the exploitation phase.
d. Variation of the search direction of the honey badger to escape from the local optima regions and to provide better opportunities for the honey badger to find the optimum prey.
e. Update the agent's position using the digging phase, where the performance of the honey badger is the same as the Cardioid shape.
f. Update the agent's position using the honey phase, where the honey badger wants to reach the beehive by following the honeyguide bird.
g. If the new position is better than the last one, then the agent position is updated using the new position.
h. After performing all iterations, display the best solution and best position.

B. ANN CONTROLLER MODEL ARCHITECTURE

The architecture used to model neural networks is MLP. An MLP network can be used as a general approximation. This implies that the aforementioned network possesses the capability to effectively estimate any smooth non-linear function with a specified level of accuracy. The amount of neurons in the network's hidden layer affects this accuracy.

TABLE 3. Control parameters from HBA and ANN.

Power Interruption		Honey Badger Algorithm (HBA)			ANN			Abs Error (%)		
MW	%	K_p	K_i	K_d	K_p	K_i	K_d	E_{Kp}%	E_{Ki}%	E_{Kd}%
50	5.00	40.81	11.34	41.67	39.94	10.75	41.46	2.07	5.20	0.48
75	7.50	39.88	10.93	41.69	39.86	10.78	41.52	0.04	1.31	0.40
100	10.0	38.79	10.76	41.70	38.80	10.93	41.94	0.03	1.50	0.56
125	12.5	36.04	11.33	42.30	35.62	11.37	42.98	1.14	0.36	1.49
150	15.0	34.12	11.78	44.38	34.64	11.61	43.34	1.42	1.38	2.29
175	17.5	34.58	11.54	43.53	34.70	11.79	43.47	0.32	1.96	0.13
200	20.0	35.46	11.47	42.16	34.75	11.22	43.29	1.96	2.12	2.49
225	22.5	34.47	8.79	40.04	33.43	8.07	38.56	2.94	8.43	3.64
250	25.0	33.38	7.58	37.15	33.84	8.11	39.17	1.29	6.23	4.91
275	27.5	34.13	7.75	40.61	34.63	8.30	40.62	1.38	6.37	0.01
300	30.0	34.78	8.54	42.76	35.89	8.73	42.39	2.94	2.00	0.83
325	32.5	38.37	10.93	44.59	37.87	10.69	44.04	1.25	2.10	1.18
350	35.0	41.13	11.59	45.88	40.71	12.20	45.12	0.98	4.80	1.60
375	37.5	42.08	14.46	38.13	41.79	14.31	38.25	0.66	0.97	0.29
400	40.0	44.72	17.79	34.48	44.61	18.01	33.84	0.25	1.16	1.79
425	42.5	45.95	21.24	35.18	46.84	21.85	36.38	1.80	2.65	3.14
450	45.0	47.87	23.66	36.62	47.45	23.29	36.34	0.84	1.53	0.72
475	47.5	41.16	23.77	30.36	41.80	23.21	28.69	1.44	2.28	5.52
500	50.0	43.28	24.47	26.35	41.32	25.01	28.86	4.50	2.06	8.25
525	52.5	41.73	27.36	31.47	41.92	28.32	31.10	0.44	3.21	1.12
550	55.0	38.39	29.82	35.42	41.58	31.38	34.95	7.28	4.73	1.27
575	57.5	40.59	33.43	37.81	40.97	33.21	38.58	0.89	0.61	1.88
600	60.0	41.63	36.85	40.56	40.48	34.06	40.72	2.69	7.76	0.37
625	62.5	40.26	34.71	41.03	40.11	34.33	41.73	0.36	1.06	1.60
650	65.0	39.48	32.89	42.84	39.24	34.12	42.30	0.56	3.42	1.23
675	67.5	37.55	33.18	44.51	36.27	33.03	43.06	3.34	0.43	3.21
700	70.0	35.18	32.09	45.88	33.93	30.39	43.95	3.51	5.31	4.17
725	72.5	31.50	27.26	43.82	30.41	27.49	44.30	3.40	0.82	1.03
750	75.0	28.10	24.45	41.96	30.27	25.41	44.23	6.81	3.59	4.89
775	77.5	29.39	22.95	42.79	30.60	23.55	43.97	3.77	2.44	2.56
800	80.0	30.70	22.48	43.82	31.22	21.54	43.56	1.58	4.15	0.56

TABLE 3. *(Continued.)* **Control parameters from HBA and ANN.**

825	82.5	32.85	19.12	43.07	32.16	19.25	42.99	2.05	0.64	0.19
850	85.0	35.84	17.10	42.24	33.55	16.75	42.16	6.46	1.98	0.18
875	87.5	37.03	14.78	40.78	35.56	14.21	40.98	3.93	3.82	0.46
900	90.0	38.42	12.03	39.57	38.25	11.89	39.28	0.42	1.13	0.70

TABLE 4. **Output of different algorithms for 50% power loss.**

Algorithms	kp	ki	kd	Fitness
PSO [43]	44.753	27.427	26.701	0.00084731
CHIMP [58]	44.646	27.338	26.645	0.00084830
HBA	45.556	25.758	27.738	0.00077717

This feature makes this structure popular in identifying non-linear systems. Here, a back-propagation approach and a tan sigmoid activation function have been utilized with a feed-forward MLP with two hidden layers and 10 neurons per layer. The schematic diagram of the proposed MLP neural network architecture is shown in Figure 11. Finally, Equation (21) shows the output of the neural network in terms of the weights of the output layer and the hidden layer. The input to the Artificial Neural Network (ANN) consists of the interrupted power P_{12}, which represents the loss of load. The ANN output is then updated using three control settings, namely K_p, K_i, and K_d.

$$\hat{y}_i(k) = \sum_{j=1}^{n_h} W_{i,j} f_j \left(\sum_{l=1}^{n_\varphi} w_{j,l} \varphi_l + w_{j,0} \right) + W_{i,0} \qquad (21)$$

where $W_{i,j}$ are the weights of the output layer, $w_{j,l}$ is the weights of the input layer, f_j is the activation function of neuron j in the hidden layer, nh is the number of neurons in the hidden layer, and $n\varphi$ is the number of neural network inputs.

C. ANN TRAINING DATA

To train this controller, we need first to produce reliable training data. As previously stated, the input to the artificial neural network (ANN) consists of the interrupted power P12, which represents the loss of load. The output of the ANN is the updated values of three control parameters, namely K_p, K_i, and K_d, which pertain to an auxiliary governor. The utilization of the Honey Badger method, a widely recognized optimization technique known for its resilience and rapid convergence, is employed to derive the PID controller parameters across various degrees of load reduction. In our case study, we considered Levels from 10 % to 100 % Load loss in steps of 10 %.

Where the mean square of error of the frequency of the over-speeding generators is minimized to obtain the corresponding optimum K_p, K_i, K_d parameters. Results can be summarized as shown in Table 2. And simulations in Figure 12 show the superiority of the HBA-based PID controller when compared to traditional and Zieglar Nicholas PID design. For example, in Figure 12(a), for 20% of load loss, the HBA method reached a steady state in less than

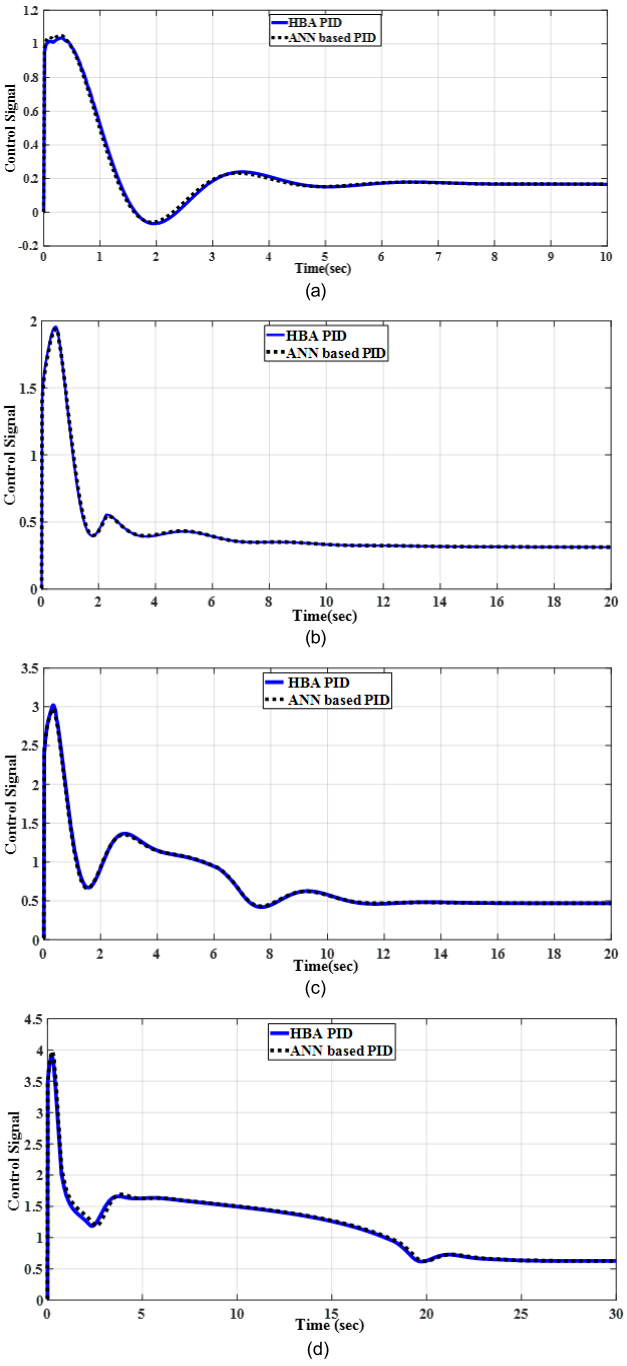

FIGURE 15. **PID controller output control signal in case 3. (a) 20% of load loss in Area 1, (b) 40% of load loss in Area 1, (c) 60% of load loss in Area 1, and (d) 80% of load loss in Area 1.**

10 seconds, while in the ZN method, the frequency is still fluctuating after 20 seconds. As you can see from other results in Figure 12(b-d), the HBA method was able to reduce the frequency overshoot from 52 Hz to the desired range of 50 Hz for a maximum of 20 seconds for different load loss percentages. Finally, Table 2 shows the results of both HBA and ZN methods, that there is an obvious difference in the choice of PID parameters between the two methods. Furthermore, Figure 12(e) shows the percentage of

TABLE 5. Sensitivity analysis of the proposed control strategy.

Changed dynamic parameter	Percentage of changes	Frequency (Hz) at 20% Power loss		Frequency (Hz) at 50% Power loss		Frequency (Hz) at 80% Power loss	
		Maximum frequency	Minimum frequency	Maximum frequency	Minimum frequency	Maximum frequency	Minimum frequency
Nominal	**0**	**50.619**	**49.953**	**51.520**	**49.690**	**50.982**	**49.670**
T_{SM}	-25%	50.580	49.958	51.489	49.757	51.951	49.640
	+25%	50.649	49.921	51.545	49.640	51.956	49.620
T_{CH}	-25%	50.580	49.957	51.460	49.665	52.220	49.558
	+25%	50.660	49.908	51.560	49.590	52.275	49.475
T_{RH}	-25%	50.625	49.910	51.520	49.750	51.905	49.558
	+25%	50.605	49.951	51.508	49.500	51.895	49.400
T_{CO}	-25%	50.618	49.955	51.509	49.455	51.962	49.620
	+25%	50.618	49.945	51.523	49.710	52.328	49.250
H	-25%	50.725	49.935	51.751	49.130	52.200	49.610
	+25%	50.559	49.950	51.385	49.700	51.953	49.590

frequency overshoot per load loss, which can be concluded by keeping the overshoot under 4% up to 80% of load loss with the HBA method. Moreover, the HBA-PID controller needs its parameters to be fine-tuned whenever the amount of the interrupted power changes to optimize the frequency response verifying the need for an adaptive neural controller that would be capable of adapting to changes in Load loss levels and provide the correct HBA optimized values for PID controller.

D. ADAPTIVE NEURAL NETWORK TRAINING

The neural network will be trained using supervised training to adjust the PID parameters to the different honey badger parameters (presented in Table 2) based on the amount of measured power loss. Moreover, ANN training methods are generally classified into two categories: first-order and second-order methods. In the first-order methods, only the first-order gradient of the criterion function is used, and in the second-order methods, the second-order gradient and the Hessian matrix are used. The algorithm used in this section will be the L-M algorithm. This algorithm, which is considered a second-order method, is one of the fastest algorithms in ANN training and is more stable than methods like Newton's algorithm. In this algorithm, to ensure the invertibility of the approximation of the Hessian matrix, a coefficient of the unit matrix called the combination coefficient is added to it. Moreover, Figure 13 shows the training process for the proposed controller.

E. VALIDATION OF ADAPTIVE NEURAL NETWORK CONTROLLER PERFORMANCE

Numerous disturbances are taken into consideration to confirm the efficacy of the suggested adaptive control approaches. The interrupted power is considered in this study to ensure the robustness of the suggested adaptive control technique. The interrupted power will be altered between 5% and 90% with a step of 2.5% (35 points). HBA obtains the PID controller parameters for each load loss (i.e., power interruption) to minimize the goal function. These parameters (K_p, K_i, K_d) are compared to the value provided by the ANN with these conditions to check online control parameters adaptation. Figure 14 shows the percentage reduction of control signal error of coefficients k_p, k_i, k_d by ANN according to the data obtained from the HBA algorithm. The purpose of using ANN is to reduce the error percentage of HBA and provide a controller whose K_p, K_i, and K_d parameters are capable of changing and adapting to different load loss conditions.

All these results are shown in Table 3. As you can see, the maximum error reduction by ANN for k_p is 7.663%, ki is 8.87% and k_d is 8.681%, which shows the good performance of the proposed controller. Moreover, a comparison is made between the control signal of the PID controller optimized with HBA and the proposed ANN for different load losses, which is shown in Figure 15. As you can see, there is a slight difference between the output of the PID controller during the two approaches of HBA and ANN.

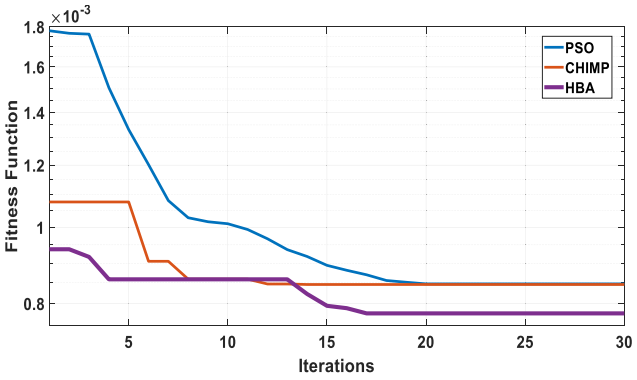

FIGURE 16. Convergence curve of fitness function for different algorithms.

Next, in Figure 16 and Table 4, to show the better performance of the HBA algorithm, a comparison with the PSO [43], and CHIMP [58] optimization algorithms has been made for 50% Power Loss. As you can see in Figure 16, the convergence curve of the fitness function obtained by the HBA algorithm has a lower value, which is shown in Table 4 of the output values of the algorithms.

TABLE 6. Evaluation and comparison of different strategies of frequency control in keeping frequency within safe limits.

Provider	Strategies	Controller type	Indexes	Features	Power system type	Maximum disturbance percentage
Nayak et al (2022) [59]	Load frequency control based on fuzzy logic	PID	ITAE, IAE, ITSE, ISE	Using the fuzzy PID controller based on adjusting the coefficients with the hybrid moth flame optimization pattern search algorithm	Two areas hydrothermal system tested in OPAL	50 %
Pathak et al (2023) [60]	Design of (FOPD-(1+FOI)) cascade controller for load frequency management	FOPD	CFD, ITAE, IAE, ITSE, ISE	Improving the implementation of automatic generation control with FOPD controller set with wild horse optimizer in such a way that control errors in feedback control loops are included in this structure.	New England IEEE 39 test bus	45 %
Pathak et al (2022) [61]	Design of ((PDF)-FOPI) controller for microgrid load frequency control	(1+PDF)-FOPI	CFD, ITAE, IAE, ITSE, ISE	Using the marine predator algorithm to optimize the proposed controller coefficients, the presence of different sources such as PV, WT, and ESE in the network	New England IEEE 39 test bus	80 %
Ramesh et al (2023) [62]	Load frequency control based on the sliding mode control	PID	Settling time, frequency deviation, MIE	Using PID controller with supplementary control (I-SMC) optimized with GTO algorithm, the presence of different sources such as DEG, and WT, in the network	Two-area	50 %
Pathak et al (2023) [63]	Design of load frequency management controller in microgrid with adjustable supplementary controller with BWOA algorithm	PIDF-(1+I)	CFD, ITAE, IAE, ITSE, ISE	Adjusting PIDF-(1+I) controller parameters with BWOA algorithm, taking into account the uncertainty of microgrid resources such as PV and WT and nonlinear system limitations, the presence of DEG, ESS in the network	New England IEEE 39 test bus	80 %
Presented	Neuro PID optimized with HBA algorithm	PID	ISE	Design of intelligent PID controller optimized with ANN-HBA hybrid algorithm based on sensitivity analysis	Two-area, four-machine system	85 %

F. SENSITIVITY ANALYSIS

In this part, to show the effect of dynamic parameters on the performance of the proposed strategy, a series of uncertainties on the parameters including governor servomotor time constant (T_{SM}), inlet steam chest (T_{CH}), Reheater time constant (T_{RH}), cross-over time constant (T_{CO}), and system

inertia (H), is considered for sensitivity analysis. To show the robustness of the proposed controller strategy, wide uncertainty according to Table 5 has been applied for the dynamic values for 20%, 50% and 80% power loss in the first area. The maximum and minimum frequency values are shown in Table 5 for parameters uncertainty (±25%). Results show that the system performance is more sensitive to the changes of system inertia (H).

Finally, in Table 6, a comparison and evaluation between some strategies presented in frequency control of multi-area systems is shown. Some criteria such as the type of strategy and proposed controller structure, indicators, characteristics of each strategy, network type, and maximum disturbance load in percentage are considered.

V. CONCLUSION

The paper shows the superiority and adaptability of Neural Network controllers when trained using proper data. It has been shown that PID controller based on recent robust optimization techniques can provide better results than traditional designs, however, such PID-optimized parameters vary as the operating condition and disturbance value varies. Here Neural Networks come in handy when trained with the aforementioned data they can adapt and change the controller parameters to the correct values once they recognize the operating condition situation. Moreover, results show that the proposed adaptable controller has the capability of keeping frequency within safe limits for disturbances reaching 85% of area load without any fluctuations in the response and with an ISE value of 7.708×10^{-4} and an MDR of 0.1237 has a favorable performance while the conventional Ziegler Nicholas controller and the traditional auxiliary high gain P controller succeed only at a maximum of 52 % and 40% of the load loss respectively. It is worth mentioning that the P controller has the extra disadvantage of introducing long-period frequency oscillations. Another suggestion to improve the proposed strategy is to use neural networks based on the predictive model with an error compensator, to increase the accuracy of the controller in addition to reducing the calculations and training data.

REFERENCES

[1] Z. A. Obaid, L. M. Cipcigan, L. Abrahim, and M. T. Muhssin, "Frequency control of future power systems: Reviewing and evaluating challenges and new control methods," *J. Modern Power Syst. Clean Energy*, vol. 7, no. 1, pp. 9–25, Jan. 2019.

[2] N. R. Babu, S. K. Bhagat, L. C. Saikia, T. Chiranjeevi, R. Devarapalli, and F. P. G. Márquez, "A comprehensive review of recent strategies on automatic generation control/load frequency control in power systems," *Arch. Comput. Methods Eng.*, vol. 30, no. 1, pp. 543–572, Jan. 2023.

[3] M. Dashtdar, A. Flah, S. M. S. Hosseinimoghadam, and A. El-Fergany, "Frequency control of the islanded microgrid including energy storage using soft computing," *Sci. Rep.*, vol. 12, no. 1, p. 20409, Nov. 2022.

[4] F. Arrigo, E. Bompard, M. Merlo, and F. Milano, "Assessment of primary frequency control through battery energy storage systems," *Int. J. Electr. Power Energy Syst.*, vol. 115, Feb. 2020, Art. no. 105428.

[5] W. Mendieta and C. A. Cañizares, "Primary frequency control in isolated microgrids using thermostatically controllable loads," *IEEE Trans. Smart Grid*, vol. 12, no. 1, pp. 93–105, Jan. 2021.

[6] H. R. Chamorro, F. R. S. Sevilla, F. Gonzalez-Longatt, K. Rouzbehi, H. Chavez, and V. K. Sood, "Innovative primary frequency control in low-inertia power systems based on wide-area RoCoF sharing," *IET Energy Syst. Integr.*, vol. 2, no. 2, pp. 151–160, Jun. 2020.

[7] K. Jiang, H. Su, H. Lin, K. He, H. Zeng, and Y. Che, "A practical secondary frequency control strategy for virtual synchronous generator," *IEEE Trans. Smart Grid*, vol. 11, no. 3, pp. 2734–2736, May 2020.

[8] W. Hu, Z. Wu, X. Lv, and V. Dinavahi, "Robust secondary frequency control for virtual synchronous machine-based microgrid cluster using equivalent modeling," *IEEE Trans. Smart Grid*, vol. 12, no. 4, pp. 2879–2889, Jul. 2021.

[9] C. Chen, X. Zhang, M. Cui, K. Zhang, J. Zhao, and F. Li, "Stability assessment of secondary frequency control system with dynamic false data injection attacks," *IEEE Trans. Ind. Informat.*, vol. 18, no. 5, pp. 3224–3234, May 2022.

[10] A. O. Aluko, D. G. Dorrell, R. P. Carpanen, and E. E. Ojo, "Heuristic secondary frequency control of AC/DC interconnected power system in a deregulated environment," in *Proc. Int. SAUPEC/RobMech/PRASA Conf.*, Jan. 2020, pp. 1–6.

[11] Y. Cheng, R. Azizipanah-Abarghooee, S. Azizi, L. Ding, and V. Terzija, "Smart frequency control in low inertia energy systems based on frequency response techniques: A review," *Appl. Energy*, vol. 279, Dec. 2020, Art. no. 115798.

[12] A. Fernández-Guillamón, E. Gómez-Lázaro, E. Muljadi, and Á. Molina-García, "Power systems with high renewable energy sources: A review of inertia and frequency control strategies over time," *Renew. Sustain. Energy Rev.*, vol. 115, Nov. 2019, Art. no. 109369.

[13] M. Kheshti, L. Ding, W. Bao, M. Yin, Q. Wu, and V. Terzija, "Toward intelligent inertial frequency participation of wind farms for the grid frequency control," *IEEE Trans. Ind. Informat.*, vol. 16, no. 11, pp. 6772–6786, Nov. 2020.

[14] C. Mu, W. Liu, and W. Xu, "Hierarchically adaptive frequency control for an EV-integrated smart grid with renewable energy," *IEEE Trans. Ind. Informat.*, vol. 14, no. 9, pp. 4254–4263, Sep. 2018.

[15] Y. Guan, J. C. Vasquez, J. M. Guerrero, Y. Wang, and W. Feng, "Frequency stability of hierarchically controlled hybrid photovoltaic-battery-hydropower microgrids," *IEEE Trans. Ind. Appl.*, vol. 51, no. 6, pp. 4729–4742, Nov. 2015.

[16] F. Liu, Y. Li, Y. Cao, J. She, and M. Wu, "A two-layer active disturbance rejection controller design for load frequency control of interconnected power system," *IEEE Trans. Power Syst.*, vol. 31, no. 4, pp. 3320–3321, Jul. 2016.

[17] M. Alharbi, M. Ragab, K. M. AboRas, H. Kotb, M. Dashtdar, M. Shouran, and E. Elgamli, "Innovative AVR-LFC design for a multi-area power system using hybrid fractional-order PI and PIDD2 controllers based on dandelion optimizer," *Mathematics*, vol. 11, no. 6, p. 1387, Mar. 2023.

[18] T. Yang, Y. Zhang, W. Li, and A. Y. Zomaya, "Decentralized networked load frequency control in interconnected power systems based on stochastic jump system theory," *IEEE Trans. Smart Grid*, vol. 11, no. 5, pp. 4427–4439, Sep. 2020.

[19] S. V. Stelmashchuk and E. D. Sherov, "Electromechanical speed control system for steam turbine generator," *IOP Conf. Ser., Mater. Sci. Eng.*, vol. 1089, no. 1, Mar. 2021, Art. no. 012014.

[20] G. S. da Silva, E. J. de Oliveira, L. W. de Oliveira, A. N. de Paula, J. S. Ferreira, and L. M. Honório, "Load frequency control and tie-line damping via virtual synchronous generator," *Int. J. Electr. Power Energy Syst.*, vol. 132, Nov. 2021, Art. no. 107108.

[21] L. Zhang, Y. Shen, L. Wang, J. Jia, and L. Wei, "Rotation speed control of the rotary valve in MWD tools based on speed feedforward compensation," *Math. Problems Eng.*, vol. 2021, pp. 1–8, Apr. 2021.

[22] R. A. Maher, I. A. Mohammed, and I. K. Ibraheem, "Polynomial based H_∞ robust governor for load frequency control in steam turbine power systems," *Int. J. Electr. Power Energy Syst.*, vol. 57, pp. 311–317, May 2014.

[23] G. Shahgholian, "Power system stabilizer application for load frequency control in hydro-electric power plant," *Int. J. Theor. Appl. Math.*, vol. 3, no. 4, p. 148, 2017.

[24] C. Zhao, U. Topcu, N. Li, and S. Low, "Design and stability of load-side primary frequency control in power systems," *IEEE Trans. Autom. Control*, vol. 59, no. 5, pp. 1177–1189, May 2014.

[25] M. A. Torres L., L. A. C. Lopes, L. A. Morán, and J. R. Espinoza, "Self-tuning virtual synchronous machine: A control strategy for energy storage systems to support dynamic frequency control," *IEEE Trans. Energy Convers.*, vol. 29, no. 4, pp. 833–840, Dec. 2014.

[26] M. Farrokhabadi, C. A. Cañizares, and K. Bhattacharya, "Frequency control in isolated/islanded microgrids through voltage regulation," *IEEE Trans. Smart Grid*, vol. 8, no. 3, pp. 1185–1194, May 2017.

[27] S. Sondhi and Y. V. Hote, "Fractional order PID controller for load frequency control," *Energy Convers. Manage.*, vol. 85, pp. 343–353, Sep. 2014.

[28] R. H. Kumar and S. Ushakumari, "Biogeography based tuning of PID controllers for load frequency control in microgrid," in *Proc. Int. Conf. Circuits, Power Comput. Technol. [ICCPCT]*, Mar. 2014, pp. 797–802.

[29] T. Mahto, H. Malik, and M. S. B. Arif, "Load frequency control of a solar-diesel based isolated hybrid power system by fractional order control using partial swarm optimization," *J. Intell. Fuzzy Syst.*, vol. 35, no. 5, pp. 5055–5061, Nov. 2018.

[30] M. Regad, M. Helaimi, R. Taleb, H. A. Gabbar, and A. M. Othman, "Fractional order PID control of hybrid power system with renewable generation using genetic algorithm," in *Proc. IEEE 7th Int. Conf. Smart Energy Grid Eng. (SEGE)*, Aug. 2019, pp. 139–144.

[31] S. Saxena and Y. V. Hote, "Internal model control based PID tuning using first-order filter," *Int. J. Control, Autom. Syst.*, vol. 15, no. 1, pp. 149–159, Feb. 2017.

[32] M. Barakat, "Novel chaos game optimization tuned-fractional-order PID fractional-order PI controller for load–frequency control of interconnected power systems," *Protection Control Modern Power Syst.*, vol. 7, no. 1, p. 16, Dec. 2022.

[33] H. Chen, L. Xiang, L. Lin, and S. Huang, "Fractional-order PID load frequency control for power systems incorporating thermostatically controlled loads," in *Proc. IEEE 4th Int. Electr. Energy Conf. (CIEEC)*, May 2021, pp. 1–6.

[34] M. R. Toulabi, M. Shiroei, and A. M. Ranjbar, "Robust analysis and design of power system load frequency control using the Kharitonov's theorem," *Int. J. Electr. Power Energy Syst.*, vol. 55, pp. 51–58, Feb. 2014.

[35] S. D. Hanwate and Y. V. Hote, "Optimal PID design for load frequency control using QRAWCP approach," *IFAC-PapersOnLine*, vol. 51, no. 4, pp. 651–656, 2018.

[36] V. P. Singh, N. Kishor, and P. Samuel, "Improved load frequency control of power system using LMI based PID approach," *J. Franklin Inst.*, vol. 354, no. 15, pp. 6805–6830, Oct. 2017.

[37] S. Jain and Y. V. Hote, "Design of fractional PID for load frequency control via internal model control and big bang big crunch optimization," *IFAC-PapersOnLine*, vol. 51, no. 4, pp. 610–615, 2018.

[38] M. K. Debnath, T. Jena, and S. K. Sanyal, "Frequency control analysis with PID-fuzzy-PID hybrid controller tuned by modified GWO technique," *Int. Trans. Electr. Energy Syst.*, vol. 29, no. 10, Oct. 2019, Art. no. e12074.

[39] S. M. S. Hosseinimoghadam, M. Dashtdar, M. Dashtdar, and H. Roghanian, "Security control of islanded micro-grid based on adaptive neuro-fuzzy inference system," *Sci. Bull., Ser. C Elect. Eng. Comput. Sci.*, vol. 82, no. 1, pp. 189–204, 2020.

[40] D. Tripathy, A. K. Barik, N. B. D. Choudhury, and B. K. Sahu, "Performance comparison of SMO-based fuzzy PID controller for load frequency control," in *Soft Computing for Problem Solving*, vol. 2. Singapore: Springer, 2019, pp. 879–892.

[41] M. Gheisarnejad, "An effective hybrid harmony search and cuckoo optimization algorithm based fuzzy PID controller for load frequency control," *Appl. Soft Comput.*, vol. 65, pp. 121–138, Apr. 2018.

[42] R. Kumar Khadanga, A. Kumar, and S. Panda, "Frequency control in hybrid distributed power systems via type-2 fuzzy PID controller," *IET Renew. Power Gener.*, vol. 15, no. 8, pp. 1706–1723, Jun. 2021.

[43] V. Kumarakrishnan, G. Vijayakumar, D. Boopathi, K. Jagatheesan, S. Saravanan, and B. Anand, "Optimized PSO technique based PID controller for load frequency control of single area power system," *Solid State Technol.*, vol. 63, no. 5, pp. 7979–7990, 2022.

[44] M. Dashtdar, A. Flah, S. M. S. Hosseinimoghadam, C. R. Reddy, H. Kotb, K. M. AboRas, and E. C. Bortoni, "Improving the power quality of island microgrid with voltage and frequency control based on a hybrid genetic algorithm and PSO," *IEEE Access*, vol. 10, pp. 105352–105365, 2022.

[45] M. Dashtdar, A. Flah, C. Z. El-Bayeh, M. Tostado-Véliz, A. Al Durra, S. H. E. A. Aleem, and Z. M. Ali, "Frequency control of the islanded microgrid based on optimised model predictive control by PSO," *IET Renew. Power Gener.*, vol. 16, no. 10, pp. 2088–2100, Jul. 2022.

[46] V. Veerasamy, N. I. A. Wahab, R. Ramachandran, A. Vinayagam, M. L. Othman, H. Hizam, and J. Satheeshkumar, "Automatic load frequency control of a multi-area dynamic interconnected power system using a hybrid PSO-GSA-tuned PID controller," *Sustainability*, vol. 11, no. 24, p. 6908, 2019.

[47] K. Kumari, G. Shankar, S. Kumari, and S. Gupta, "Load frequency control using ANN-PID controller," in *Proc. IEEE 1st Int. Conf. Power Electron., Intell. Control Energy Syst. (ICPEICES)*, Jul. 2016, pp. 1–6.

[48] M. K. Debnath, R. Agrawal, S. R. Tripathy, and S. Choudhury, "Artificial neural network tuned PID controller for LFC investigation including distributed generation," *Int. J. Numer. Model., Electron. Netw., Devices Fields*, vol. 33, no. 5, Sep. 2020, Art. no. e2740.

[49] A. Safari, F. Babaei, and M. Farrokhifar, "A load frequency control using a PSO-based ANN for micro-grids in the presence of electric vehicles," *Int. J. Ambient Energy*, vol. 42, no. 6, pp. 688–700, Apr. 2021.

[50] N. Calik, F. Güneş, S. Koziel, A. Pietrenko-Dabrowska, M. A. Belen, and P. Mahouti, "Deep-learning-based precise characterization of microwave transistors using fully-automated regression surrogates," *Sci. Rep.*, vol. 13, no. 1, p. 1445, Jan. 2023.

[51] S. Simon, G. M. Schwarz, A. Aichmair, B. J. H. Frank, A. Hummer, M. D. DiFranco, M. Dominkus, and J. G. Hofstaetter, "Fully automated deep learning for Knee alignment assessment in lower extremity radiographs: A cross-sectional diagnostic study," *Skeletal Radiol.*, vol. 51, no. 6, pp. 1249–1259, Jun. 2022.

[52] S. Safiullah, A. Rahman, S. A. Lone, S. M. S. Hussain, and T. S. Ustun, "Robust frequency–voltage stabilization scheme for multi-area power systems incorporated with EVs and renewable generations using AI based modified disturbance rejection controller," *Energy Rep.*, vol. 8, pp. 12186–12202, Nov. 2022.

[53] M. Kumar, S. Prasad, M. R. Ansari, and B. Mohapatra, "Resonance attacks detection and mitigation control scheme on frequency regulation in multi-area smart grid," *Int. J. Control*, vol. 96, no. 9, pp. 2212–2229, Sep. 2023.

[54] K. Akter, L. Nath, T. A. Tanni, A. S. Surja, and Md. S. Iqbal, "An improved load frequency control strategy for single & multi-area power system," in *Proc. Int. Conf. Advancement Electr. Electron. Eng. (ICAEEE)*, Feb. 2022, pp. 1–6.

[55] S. D. Al-Majidi, M. Kh. AL-Nussairi, A. J. Mohammed, A. M. Dakhil, M. F. Abbod, and H. S. Al-Raweshidy, "Design of a load frequency controller based on an optimal neural network," *Energies*, vol. 15, no. 17, p. 6223, Aug. 2022.

[56] T. Ali, S. A. Malik, I. A. Hameed, A. Daraz, H. Mujlid, and A. T. Azar, "Load frequency control and automatic voltage regulation in a multi-area interconnected power system using nature-inspired computation-based control methodology," *Sustainability*, vol. 14, no. 19, p. 12162, Sep. 2022.

[57] F. A. Hashim, E. H. Houssein, K. Hussain, M. S. Mabrouk, and W. Al-Atabany, "Honey badger algorithm: New metaheuristic algorithm for solving optimization problems," *Math. Comput. Simul.*, vol. 192, pp. 84–110, Feb. 2022.

[58] M. Khishe and M. R. Mosavi, "Chimp optimization algorithm," *Expert Syst. Appl.*, vol. 149, Jul. 2020, Art. no. 113338.

[59] P. C. Nayak, R. C. Prusty, and S. Panda, "Adaptive fuzzy approach for load frequency control using hybrid moth flame pattern search optimization with real time validation," *Evol. Intell.*, pp. 1–16, Nov. 2022, doi: 10.1007/s12065-022-00793-0.

[60] P. K. Pathak and A. K. Yadav, "Design of optimal cascade control approach for LFM of interconnected power system," *ISA Trans.*, vol. 137, pp. 506–518, Jun. 2023.

[61] P. K. Pathak, A. K. Yadav, S. Padmanaban, and I. Kamwa, "Fractional cascade LFC for distributed energy sources via advanced optimization technique under high renewable shares," *IEEE Access*, vol. 10, pp. 92828–92842, 2022.

[62] M. Ramesh, A. K. Yadav, and P. K. Pathak, "Artificial gorilla troops optimizer for frequency regulation of wind contributed microgrid system," *J. Comput. Nonlinear Dyn.*, vol. 18, no. 1, Jan. 2023, Art. no. 011005.

[63] P. K. Pathak, A. K. Yadav, A. Shastri, and P. A. Alvi, "BWOA assisted PIDF-(1+I) controller for intelligent load frequency management of standalone micro-grid," *ISA Trans.*, vol. 132, pp. 387–401, Jan. 2023.

AHMED H. YAKOUT received the bachelor's and master's degrees from the Electrical Power and Machines Department, Faculty of Engineering, Ain Shams University, Cairo, Egypt, in 2000 and 2005, respectively, and the Ph.D. degree in electrical engineering from the University of Strathclyde, Glasgow, U.K., in 2010. He is currently an Associate Professor with the Faculty of Engineering, Ain Shams University. His main research interests include electrical power systems analysis, stability, artificial intelligence, optimization, smart grid, fuzzy control, and adaptive control.

MASOUD DASHTDAR research interests include distribution systems, including fault diagnosis in power systems, artificial neural network computing, power electronics, electric machines, renewable energy, microgrid, smart grids, harmonic analysis, power quality, optimization, and metaheuristic algorithms. In 2023, according to the AD Scientific Index database, he was ranked 534,858 among 1,353,358 scientists in his field, which is one of the Top 10% of Scientists in the specified subject. He is currently a Reviewer of ISI journals, including *Journal of Electrical Engineering and Technology* (JEET), *Artificial Intelligence Review*, *Soft Computing*, *Electrical Engineering*, *Iranian Journal of Science and Technology*, *Transactions of Electrical Engineering*, *Sustainable Energy, Grids and Networks*, *International Transactions on Electrical Energy Systems*, *Canadian Journal of Electrical and Computer Engineering*, IEEE Access, and IEEE Transactions on Circuits and Systems—II cooperation.

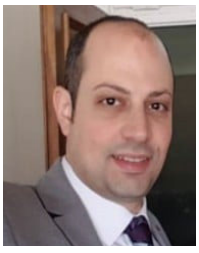

KAREEM M. ABORAS received the B.Sc., M.Sc., and Ph.D. degrees in electrical engineering from the Faculty of Engineering, Alexandria University, Alexandria, Egypt, in 2010, 2015, and 2020, respectively. Currently, he is an Assistant Professor with the Electrical Power and Machines Department, Faculty of Engineering, Alexandria University. His Ph.D. research work is focused on the performance enhancement of renewable energy conversion systems. His research interests include power electronics, control, drives, power systems, and renewable energy systems. He is a reviewer of IET journal.

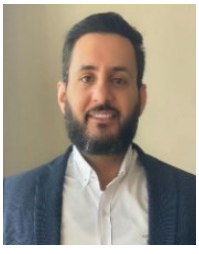

YAZEED YASIN GHADI received the Ph.D. degree in electrical and computer engineering from The University of Queensland. He is currently an Assistant Professor of software engineering with Al Ain University. Before joining Al Ain University, he was a Postdoctoral Researcher with The University of Queensland. He has published more than 25 peer-reviewed journals and conference papers and he holds three pending patents. His current research interests include developing novel electro-acoustic-optic neural interfaces for large-scale high-resolution electrophysiology and distributed optogenetic stimulation. He was a recipient of several awards. His dissertation on developing novel hybrid plasmonic photonic on-chip biochemical sensors received the Sigma Xi Best Ph.D. Thesis Award.

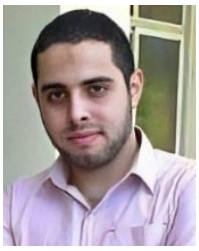

AHMED ELZAWAWY received the M.Sc. and Ph.D. degrees in electrical engineering from the Faculty of Engineering at Shoubra, Department of Electrical Engineering, Benha University, Egypt, in 2015 and 2020, respectively. He is currently a Lecturer with the Faculty of Engineering at Shoubra, Benha University. His research interests include power system stability and control, renewable energy technology, and microgrids.

AMR YOUSEF (Member, IEEE) received the B.Sc. and M.Sc. degrees from the Engineering Mathematics Department and the Electrical Engineering Department, Alexandria University, in 2001 and 2006, respectively, and the Ph.D. degree in electrical and computer engineering from Old Dominion University (ODU), in May 2012. He was a Postdoctoral Research Associate with the Old Dominion Vision Laboratory, USA. He is currently an Assistant Professor with the Electrical Engineering Department, University of Business and Technology, Saudi Arabia. His research interests include optimization techniques, image processing/computer vision, and machine learning algorithms. He is a member of SPIE and OSA.

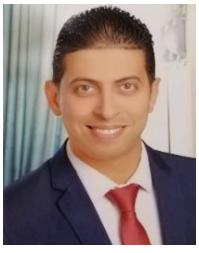

HOSSAM KOTB received the B.Sc., M.Sc., and Ph.D. degrees in electrical engineering from the Faculty of Engineering, Alexandria University, Alexandria, Egypt, in 2009, 2013, and 2020, respectively. Currently, he is an Assistant Professor with the Electrical Power and Machines Department, Faculty of Engineering, Alexandria University. His Ph.D. research work is focused on the performance enhancement of renewable energy conversion systems. His research interests include power system analysis, electrical drives, modern control techniques, smart grids, optimization, electric vehicles, and renewable energy systems. He is an Associate Editor of *Alexandria Engineering Journal* (AEJ).